Mon. Not. R. Astron. Soc. **000**, 1–12 (2011) Printed 4 July 2011 (MN LaTeX style file v2.2)

arXiv:1107.0180v1 [astro-ph.HE] 1 Jul 2011

Varying disc–magnetosphere coupling as the origin of pulse profile variability in SAX J1808.4–3658

Jari J. E. Kajava,[1⋆] Askar Ibragimov,[1,2] Marja Annala,[1] Alessandro Patruno[3] and Juri Poutanen[1⋆]
[1]*Astronomy Division, Department of Physics, P.O.Box 3000, FI-90014 University of Oulu, Finland*
[2]*Sabancı University, Orhanlı-Tuzla, Istanbul, 34956, Turkey*
[3]*Astronomical Institute "Anton Pannekoek," University of Amsterdam, Kruislaan 403, 1098 SJ Amsterdam, The Netherlands*

Accepted 2011 June 30. Received 2011 June 30; in original form 2011 March 23

ABSTRACT

Accreting millisecond pulsars show significant variability of their pulse profiles, especially at low accretion rates. On the other hand, their X-ray spectra are remarkably similar with not much variability over the course of the outbursts. For the first time, we have discovered that during the 2008 outburst of SAX J1808.4–3658 a major pulse profile change was accompanied by a dramatic variation of the disc luminosity at almost constant total luminosity. We argue that this phenomenon is related to a change in the coupling between the neutron star magnetic field and the accretion disc. The varying size of the pulsar magnetosphere can influence the accretion curtain geometry and affect the shape and the size of the hotspots. Using this physical picture, we develop a self-consistent model that successfully describes simultaneously the pulse profile variation as well as the spectral transition. Our findings are particularly important for testing the theories of accretion onto magnetized neutron stars, better understanding of the accretion geometry as well as the physics of disc-magnetosphere coupling. The identification that varying hotspot size can lead to pulse profile changes has profound implications for determination of the neutron star masses and radii.

Key words: accretion, accretion discs – pulsars: individual: SAX J1808.4–3658 – stars: neutron – X-rays: binaries

1 INTRODUCTION

SAX J1808.4–3658 was first detected with the Wide Field Cameras on board the *BeppoSAX* satellite in 1996 (in 't Zand et al. 1998). In 1998, another outburst of SAX J1808.4–3658 was observed with *Rossi X-ray Timing Explorer* (*RXTE*) and the discovery of ≈ 401 Hz pulsations led to its identification as the first accreting millisecond pulsar (AMP; Wijnands & van der Klis 1998; Chakrabarty & Morgan 1998). Since 1998, the source has been in outburst roughly every 2.5 years (2000, 2002, 2005 and 2008). During the outbursts of SAX J1808.4–3658 (and other AMPs), the magnetic field of the neutron star (NS) channels the accreted matter on to the stellar magnetic poles. The emitted radiation from these hotspots is then modulated at the stellar spin period, that results in coherent pulsations. In a typical outburst of SAX J1808.4–3658 (see fig.2 in Hartman et al. 2008) the source rises from quiescence in roughly five days, reaching a peak flux of about $2 \times 10^{-9}\,\mathrm{erg\,cm^{-2}\,s^{-1}}$ in the 2–25 keV range of the *RXTE* Proportional Counter Array (PCA). After the peak, the source flux drops slowly ("slow decay" stage) in the course of the next ten days, although the 2008 outburst had a double peaked light curve (Hartman et al. 2009). The slow decay stage is followed by the "rapid drop" stage, where the flux drops by an order of magnitude in a couple of days after which the source exhibits several re-brightening episodes every five days or so ("flaring tail" stage, see also Patruno et al. 2009b, Ibragimov & Poutanen 2009).

The system parameters of SAX J1808.4–3658 are the best known among AMPs. The orbital period is $\approx$ 2 hours (Chakrabarty & Morgan 1998; Burderi et al. 2009; Hartman et al. 2009) and the companion star has a very low mass of $M_{\rm c} \sim 0.05\mathrm{M}_{\odot}$ (Bildsten & Chakrabarty 2001). The analysis of type I X-ray bursts by Galloway & Cumming (2006) gave a distance estimate of 3.5 ± 0.1 kpc. The inclination has been constrained to i =36°–67° using optical observations (Deloye et al. 2008) and the X-ray analysis (Ibragimov & Poutanen 2009) of the 2002 outburst led to a similar constraint of $i \approx 50°–70°$. By studying the long term timing evolution of the system, Hartman et al. (2008) constrained the neutron star surface magnetic dipole field to a range of $B_{\rm S} = (0.4–1.5) \times 10^8$ G. Another estimate of $B_{\rm S} = (0.8 \pm 0.5) \times 10^8 k_{\rm A}^{-7/4}$ G from pulse profile variability, was derived by Ibragimov & Poutanen (2009), where the factor $k_{\rm A} \approx 0.5$ (Long et al. 2005). Also, Burderi et al. (2006) gave an estimate of $B_{\rm S} \sim (3.5 \pm 0.5) \times 10^8$ G and Patruno et al. (2009c) obtained $B_{\rm S} = (2–3) \times 10^8$ G.

⋆ E-mail: jari.kajava@oulu.fi, juri.poutanen@oulu.fi

The energy spectra of SAX J1808.4–3658 has been studied extensively (e.g. Gilfanov et al. 1998; Gierliński et al. 2002; Poutanen & Gierliński 2003; Ibragimov & Poutanen 2009). It was pointed out already by Gilfanov et al. (1998) that the spectral shape remains remarkably similar when flux changes by more than an order of magnitude throughout the outburst. The energy spectrum is roughly flat (photon index $\Gamma \approx 2$) with a cutoff/roll-over at energies above ~ 50 keV. Such spectra – also seen in other AMPs (Poutanen 2006) – are most likely produced by thermal Comptonization of soft seed photons originating from the heated stellar surface by hot electrons in the accretion shock (Gierliński et al. 2002; Poutanen & Gierliński 2003; Ibragimov & Poutanen 2009). Below ~ 5 keV an additional $T \approx 0.5$ keV thermal component is visible that is associated with the heated surface of the NS. *XMM-Newton* observations have revealed another *non-pulsating* cooler thermal component due to the accretion disc (Patruno et al. 2009a). The X-ray emission from the NS surface irradiates the accretion disc, that causes spectral hardening above 10 keV due to Compton reflection (Ibragimov & Poutanen 2009). This irradiation also produces an iron line at 6.4 keV and the modelling of the line profiles from *XMM-Newton* and *Suzaku* observations by Papitto et al. (2009) and Cackett et al. (2009) has given tight constraints on inclination and the accretion disc truncation radius. We note, however, that these results depend strongly on the continuum spectral model and data reduction issues (see Ng et al. 2010, for discussion).

Although many aspects of AMP physics are known, one of the unresolved puzzles is the origin of sudden pulse profile changes in SAX J1808.4–3658 (Hartman et al. 2008, 2009) and other AMPs. There are many mechanisms that can cause such changes (Poutanen 2008) and they contribute to the “timing noise” seen in many AMPs (e.g. Burderi et al. 2006; Papitto et al. 2007; Riggio et al. 2008; Patruno et al. 2009c; Poutanen et al. 2009). One of these remarkable pulse profile changes occurred in the 2008 outburst of SAX J1808.4–3658 (Hartman et al. 2009). In the beginning of the slow decay stage, the pulse profile was rather symmetric showing only small harmonic content. However, on September 27 the fundamental pulse amplitude decreased by almost 50 per cent, while no change was seen in other observed quantities, especially the observed flux and phases of the harmonics. A few days later on October 2 (MJD 54742), the pulse profile quickly morphed to have two peaks. This time the pulse profile transition was accompanied by a decay in the observed flux and jumps in pulse phases. The double peaked profile was seen only for about three days, because on October 6 (MJD 54746), right before the onset of the rapid drop stage, the fundamental amplitude increased significantly and the profile changed again to a shape similar to what was seen before September 27. This behaviour cannot be explained by a change in the accretion disc truncation radius that was suggested by Ibragimov & Poutanen (2009) and Poutanen et al. (2009). Although this model explains the jump in the fundamental phase (and the pulse profile change), that is associated with the rapid drop stage of the 2002 outburst of SAX J1808.4–3658 (Burderi et al. 2006), it cannot be the case here simply because the observed flux (which can be related to the truncation radius) in these sudden pulse profile changes is almost an order of magnitude higher and it remains nearly constant (see fig. 1 in Hartman et al. 2009). Among the 13 known AMPs (see Patruno 2010a, and references therein), some sources show similar jumps in the fundamental pulse amplitudes as in the 2008 outburst of SAX J1808.4–3658. A few examples include XTE J0929–314 (Galloway et al. 2002), the first eclipsing AMP SWIFT J1749.4–2807 (Markwardt & Strohmayer 2010; Altamirano et al. 2011) and SWIFT J1756.9–2508 (Patruno et al. 2010a). Also, similar jumps in the fundamental pulse amplitude was seen in the 2002 and 2005 outbursts of SAX J1808.4–3658 (see fig. 6 in Ibragimov & Poutanen 2009 and fig. 1 in Hartman et al. 2008).

The variability in pulse amplitudes and profiles are sometimes accompanied with jumps in pulse phases (Papitto et al. 2007; Riggio et al. 2008; Patruno et al. 2009c). In most cases, this timing noise is related with changes in the observed flux (Burderi et al. 2006; Ibragimov & Poutanen 2009; Patruno et al. 2009c) and the most notable changes usually occur in the fundamental phase (Burderi et al. 2006; Papitto et al. 2007; Riggio et al. 2008; Patruno et al. 2009c). This type of timing noise is most likely caused by mass accretion rate dependent change of the hotspot location on the NS surface (Lamb et al. 2009), which explains the overall trends with flux and pulse phase residuals in SAX J1808.4–3658 (Hartman et al. 2008) and in many other AMPs (Patruno et al. 2009c). However, although the general trends can be explained (Patruno et al. 2009c), there are several AMPs where additional timing noise is clearly present. Most notable cases are the 2002, 2005 and 2008 outbursts of SAX J1808.4–3658, XTE J1807–294 and XTE J0929–314 (see fig. 3 in Patruno et al. 2009c and fig. 1 in Hartman et al. 2009). In these cases another mechanism – that is not related to changes in mass accretion rate – must be responsible for the timing noise.

In this paper, we present our spectral and timing analysis of the 2008 outburst of SAX J1808.4–3658 using *Swift* and *RXTE* data. We find evidence that the sudden changes in the pulse profiles and in pulse amplitudes of SAX J1808.4–3658 are driven by a changing interaction between the NS magnetic field and the accretion disc.

2 OBSERVATIONS AND DATA REDUCTION

The 2008 outburst of SAX J1808.4–3658 was first detected on September 21 (Markwardt & Swank 2008). The outburst was very similar to the 2005 outburst in duration and brightness, albeit the flaring stage was dimmer (Hartman et al. 2009). The slow decay stage of the outburst outburst was monitored by both *Swift* and *RXTE* from September 24 to October 3, during which the fundamental pulse amplitude and the pulse profile changed significantly (see Hartman et al. 2009, fig. 1). In this paper we perform a detailed spectral and pulse profile analysis of these data in order to investigate the origin of this sudden timing transition.

The *RXTE* data (ObsID 93027) were reduced using HEASOFT v.6.8 and the CALDB. We used data taken both by *RXTE*/PCA (3–25 keV) and HEXTE (25–100 keV). In cases where HEXTE exposures were short, we ignored the noisy channels above ~ 60 keV. Standard 0.5 per cent systematic was applied to the PCA spectra (Jahoda et al. 2006). To keep the calibration uniform, we used data from PCU 2 only (all layers). The *Swift*/XRT data (0.6–7 keV) were reduced using the XRTPIPELINE v.0.12.3 in HEASOFT v.6.8. The observations were performed in window-timing mode. We used standard filtering and screening criteria for the event selection. Exposure maps were generated with the XRTEXPOMAP task and the ancillary response files with XRTMKARF to account for different extraction regions (we used circular regions of 20 pixel radius), vignetting and psf corrections. The redistribution matrices (v.011) were taken from the CALDB. The XRT spectra were then grouped using GRPPHA to have at least 20 counts in each bin.

We used the *Swift*/XRT data to model the time averaged spectra together with the quasi-simultaneous *RXTE* pointings. There were a few cases where we could not use all the XRT data. The

Table 1. The observation log.

#	ObsID	Date and time	Exposure[a]
1	93027-01-01-07[b]	2008-09-24 19:33:52–20:16:32	2333/763
2	00325827000[c]	2008-09-24 21:28:45–21:56:00	...
3	00030034026	2008-09-24 23:17:40–23:32:00	816
4	93027-01-01-06	2008-09-25 05:24:48–06:24:32	1035/414
5	93027-01-01-05	2008-09-25 08:08:32–10:44:00	6482/2359
6	00030034027	2008-09-25 13:34:28–13:52:00	1005
7	93027-01-01-10	2008-09-25 19:52:16–20:36:32	490/123
8	00030034028	2008-09-26 11:59:49–12:19:00	1142
9	93027-01-02-00	2008-09-26 13:55:28–18:06:40	9713/3264
10	93027-01-02-01	2008-09-26 23:32:16–23:50:40	1060/356
11	00030034029	2008-09-27 04:04:15–04:23:00	1116
12	93027-01-02-05	2008-09-27 10:24:00–15:00:32	8942/3411
13	93027-01-02-06	2008-09-28 05:24:32–05:57:52	1943/668
14	00030034030[d]	2008-09-28 12:11:35–15:44:00	880
15	93027-01-02-03	2008-09-28 16:13:52–17:35:44	3201/1043
16	93027-01-02-04	2008-09-29 06:22:08–07:45:36	2775/1022
17	00030034031	2008-09-29 10:44:25–10:59:00	849
18	00030034032[e]	2008-09-30 01:12:05–01:33:00	...
19	93027-01-02-07	2008-09-30 09:03:12–10:01:36	3181/1154
20	93027-01-02-09	2008-09-30 14:01:04–15:03:44	2306/744
21	93027-01-02-02	2008-10-01 11:44:48–14:59:12	6637/2242
22	00030034033	2008-10-01 14:25:42–14:45:00	1131
23	93027-01-02-08	2008-10-02 14:25:52–17:19:44	6280/2035
24	00030034034[f]	2008-10-02 22:23:50–23:59:59	848
25	93027-01-03-00	2008-10-03 09:49:20–13:22:40	7557/2510

[a] XRT or PCA/HEXTE exposure times (in seconds). [b] Only data before X-ray burst used. [c] Not used due to proximity to the X-ray burst. [d] Only data from snapshot 2 used. [e] Not used because the source was right on top of bad columns. [f] Only data from snapshot 1 used.

first XRT observation (observation 2, see Table 1) was triggered by an X-ray burst. We found that the XRT spectrum differed from the PCA spectrum taken before the X-ray burst and also from the XRT spectrum taken only 3 hours after the X-ray burst (observation 3). The spectra of observations 1 and 3 matched well indicating that the first XRT spectra was affected by the X-ray burst and it was therefore excluded from the analysis. Also, we did not use the observation 18, because the source was right on top of the bad columns. In two occasions, where XRT observations were split into two snapshots (14 and 24), we used the data from the longer snapshot.

3 SPECTRAL AND TIMING ANALYSIS

3.1 Simultaneous timing- and spectral transition

During the slow decay stage of the 2008 outburst – on September 27 (MJD 54736) – the pulse amplitude dropped and the pulse profile changed significantly (see Hartman et al. 2009, fig. 1). The origin of these type of timing changes is not well understood, but they must be caused by some changes in the accretion geometry. In order to analyse this timing transition, we construct pulse profiles at various energies and different time intervals using ephemeris from Hartman et al. (2009). The observed pulse profiles are then fitted by a sum of two harmonics:

$$F(\phi) = \bar{F}\{1 + a_1 \cos[2\pi(\phi - \phi_1)] + a_2 \cos[4\pi(\phi - \phi_2)]\}, \quad (1)$$

where $F(\phi)$ is the flux at phase ϕ, $\bar{F}$ is the mean flux and a_1, a_2, ϕ_1 and ϕ_2 are the amplitudes and phases of the fundamental and the first overtone, respectively. The best-fitting amplitudes and phases are presented in Fig. 1 for the soft (3.7–5.7 keV) and hard (9.8–23.2 keV) energy bands. We selected these two bands because in the hard band we have emission only from the Comptonized component, whereas in the soft band there is a contribution from the blackbody component (e.g. Ibragimov & Poutanen 2009). We see a drop in the fundamental amplitude and a change in the pulse profile on September 27 (MJD 54736), but we do not detect significant jumps in the pulse phases during the transition.

However, we find that the timing transition was accompanied with a simultaneous softening of the energy spectrum below ~ 5 keV. This can be seen by taking a ratio of the observed spectra before and after the timing transition (from XRT observations 11 and 14 and PCA observations 10 and 12). The ratio spectra are shown in Fig. 2 and the softening is clearly seen in the *Swift* as well as in the *RXTE*/PCA data. The fact that the timing- and spectral transition occur simultaneously suggests a common physical origin, so a detailed broad band spectral analysis and pulse profile modelling of this transition is warranted.

3.2 Spectral model

We modelled the spectra using XSPEC 12 (Arnaud 1996). Errors are quoted at the 90% confidence level and the errors in the fluxes were computed with the CFLUX model in XSPEC. The reported luminosities are bolometric (calculated in the range of 0.01–500 keV from the best-fitting model) assuming a distance of $D = 3.5$ kpc (Galloway & Cumming 2006).

Our spectral model consist of CONSTANT × WABS × (DISKBB + BBODYRAD + DISKLINE + COMPPS). The spectral model is rather complex and has a large number of parameters. The CONSTANT model component accounts for the different instrument normalizations between *Swift*/XRT, *RXTE*/PCA and HEXTE. We fixed the normalization of PCA and allowed XRT and HEXTE normalizations to vary. For XRT, the normalizations varied in a tight range around 0.9 between the different exposures, whereas HEXTE normalizations varied in the range of $0.52 - 0.62$. The effect of interstellar absorption was taken into account using the WABS model (Morrison & McCammon 1983), which is parametrized by the absorption column $N_{\rm H}$. We modelled the accretion disc component with the DISKBB model (Mitsuda et al. 1984), which has two parameters; the inner disc temperature $T_{\rm disc}$ and normalization (proportional to inner disc radius $R_{\rm disc}$) $K_{\rm disc} = [(R_{\rm disc}/{\rm km})/(D/10~{\rm kpc})]^2 \cos i$. For the thermal emission from the NS surface, we used the BBODYRAD model, which is characterized by the black body temperature $T_{\rm bb}$ and normalization (proportional to the surface area) $K_{\rm bb} = [(R_{\rm bb}/{\rm km})/(D/10~{\rm kpc})]^2$, where $R_{\rm bb}$ is the apparent black body radius as observed from infinity. Model COMPPS (Poutanen & Svensson 1996) – characterizing Comptonization in the accretion column (we assumed slab geometry) – is described by the following parameters: Thomson optical depth τ across the slab, electron temperature $T_{\rm e}$, seed photon temperature $T_{\rm seed}$ for Comptonization, and normalization (proportional to the surface area) $K_{\rm seed} = [(R_{\rm seed}/{\rm km})/(D/10~{\rm kpc})]^2$, with $R_{\rm seed}$ corresponding to the size of the accretion column. The Compton reflection component (included in COMPPS) is defined by the amplitude $\Re = \Omega/2\pi$ (where Ω is the solid angle covered by the cold reflector as viewed from the X-ray emitting hotspots), index α of the radial profile of the disc emissivity ($\propto r^{\alpha}$), inner- and outer disc radius, inclination i and the iron line energy and normalization $K_{\rm Fe}$ (DISKLINE, Fabian et al. 1989). We note that the DISKLINE model inner disc radius can be substantially different

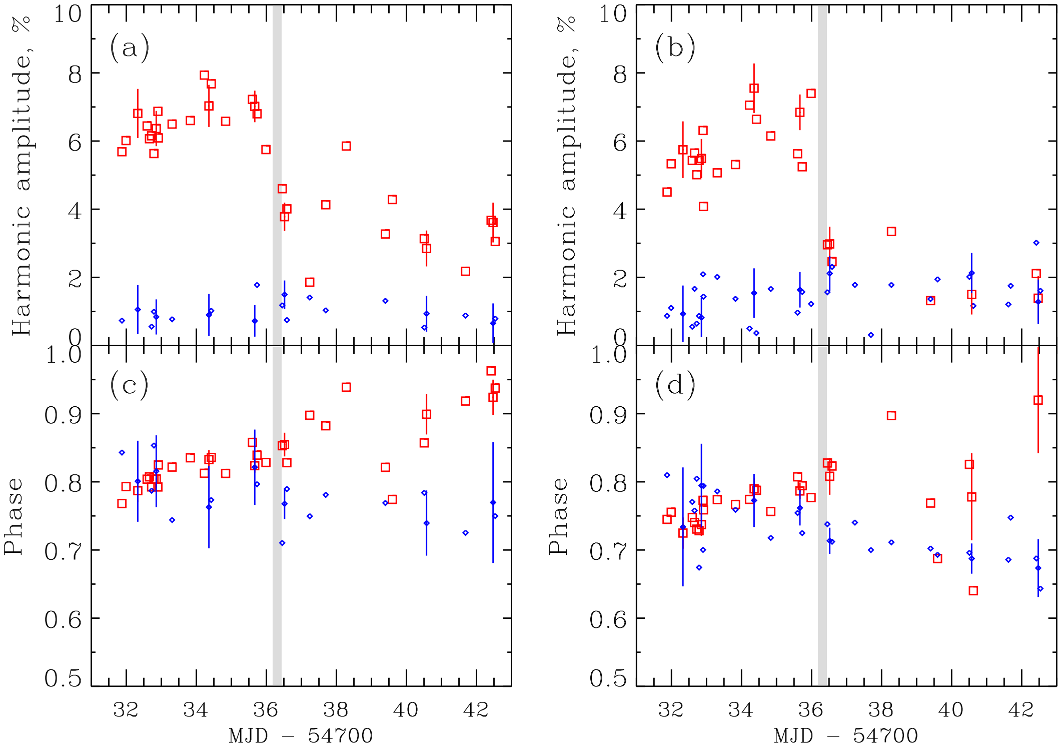

Figure 1. Change of the pulse profile parameters during the outburst. Left panels are for the soft (3.7–5.7 keV) band, while the right panels are for the hard (9.8–23.2 keV) band. Upper panels present amplitudes of the fundamental (red squares) and of the first overtone (blue diamonds). Lower panels correspond to the pulse phases shown by the same symbols. Only those phases and amplitudes that can be constrained are plotted, and errors for only a few representative data points are plotted for visual clarity. The time of the spectral transition is marked with the grey shaded strip (see Fig. 2). Note the absence of a pulse phase shift during the transition (MJD 54736).

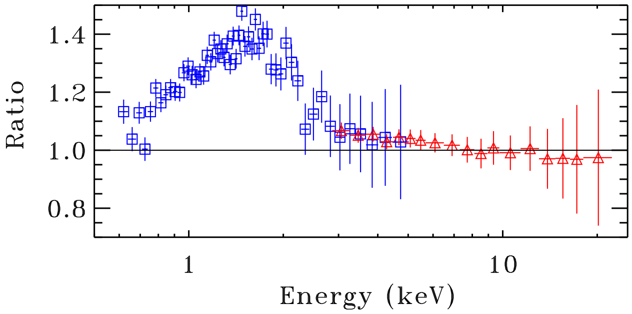

Figure 2. Ratio of the spectra from observations after and before the timing transition. The corresponding XRT spectra are from observations 14 and 11 (blue squares) and the PCA spectra are from observations 12 and 10 (red triangles). The spectral data are binned for visual clarity. The spectral transition occurred between 2008-09-27 04:23:00 and 2008-09-27 10:24:00 (see Table 1). The increase of the flux is most evident below ∼ 3 keV, where the accretion disc component dominates (see Patruno et al. 2009a and Fig. 4).

from $R_{\rm disc}$, which we derive from the DISKBB model normalization. The former is related to the disc truncation radius $R_{\rm t}$, whereas the latter traces the radius where the dissipation ceases, which is related to the magnetospheric radius $R_{\rm m}$ (see end of Section 3.3).

When we attempted to fit all these parameters to the data, we found several unphysical changes in the best-fitting parameters throughout the outburst. Most notable inconsistencies were variable inclination i and a larger hotspot radius than a typical NS radius. Furthermore, several parameters showed tight correlated changes among them. $T_{\rm e}$, τ and $\Re$ – which together define the spectral slope above ∼10 keV – were strongly correlated, resulting in large uncertainties in these parameters. Also, $N_{\rm H}$ showed inconsistent changes during the outburst. We thus had to fix several parameters to obtain reasonable values. We did this in an iterative manner, where we fixed certain parameters, then fitted the data again, inspected the results and then fixed more parameters if necessary.

Initially we fixed five parameters. Inclination was fixed to $i = 60^{\circ}$ (for both reflection and iron line, as in Ibragimov & Poutanen 2009). The inner disc radius that affects both the smearing of the line and Compton reflection was fixed to a value of $10R_{\rm S}$, where $R_{\rm S} = 2GM/c^2$ is the Schwarzschild radius. The outer disc radius was fixed to $1000R_{\rm S}$. The radial disc emissivity for reflection was fixed to $\alpha = -3$. Also, because of poor energy resolution of PCA and poor statistics of XRT spectra in the iron line region, we fixed the iron line energy to 6.4 keV.

The model as such described the data very well (the best-fitting parameters and fitting statistics were compatible to the “final results” presented in Table 2). However, as discussed in Gierliński & Poutanen (2005) and Ibragimov & Poutanen (2009), the hotspot surface area ($\propto K_{\rm bb}$) was poorly constrained and in many cases resulted in large and unphysical values. Furthermore, some residuals were present in the XRT data around 2 keV, where the calibration is known to have problems because of the Si Kα edge at 1.839 keV (Godet et al. 2009). These residuals created a problem in the fitting, because the flux contribution of the $T_{\rm bb}$ ≈0.5–0.6 keV NS blackbody component and the $T_{\rm disc}$ ≈0.3–0.4 keV disc component was very similar at this energy. We identified two cases (6 and 11) – where the XRT observations were about $3'$ off-axis – in which these instrumental residuals were the main reason why $T_{\rm disc}$, $K_{\rm disc}$, $T_{\rm bb}$, $K_{\rm bb}$ and $N_{\rm H}$ seemed to change in a correlated way during the outburst. The best-fitting value of $N_{\rm H}$ varied roughly in a range of (0.9–0.95)±0.15×10^{21} $\rm cm^{-2}$ for most of the observations, except in these two cases where it dropped to a value of $\sim (0.7 \pm 0.05) \times 10^{21}\ \rm cm^{-2}$. As we do not expect $N_{\rm H}$ to vary and its value was tightly correlated with the parameters of the accretion disc ($T_{\rm disc}$ and $K_{\rm disc}$), we fixed this parameter to the Galactic value of $1.13 \times 10^{21}\ \rm cm^{-2}$ (obtained from the HEADAS tool NH) to avoid spurious changes in the disc parameters. Also, following Ibragimov & Poutanen (2009), we set $K_{\rm bb} = K_{\rm seed}$ in the fitting, which helped to remove the correlation between $T_{\rm bb}$ and $T_{\rm disc}$ described above.

After another round of spectral fitting, we found that $T_{\rm e}$ ≈(45–55)±10 keV in all the spectral fits. In some cases the spectra were very noisy above ∼60 keV and some small changes in $T_{\rm e}$ and τ between different observations were identified to be caused by one or two spectral channels only. As we did not see any statistically important trend between the observations, we fixed $T_{\rm e}$= 50 keV, which was the best-fitting constant value. We then fitted the data again, and got physically acceptable values for all the model parameters. We also checked, that the removal of XRT data in the 1.6–2.4 keV range did not change the best-fitting parameters significantly.

3.3 Results of the spectral modelling

The time evolution of the best-fitting parameters of the spectral modelling are presented in Fig. 3 and Table 2. It is immediately obvious that there is a clear transition in the best-fitting spectral parameters on September 27 (MJD 54736), exactly when the timing transition also occurs. However, we emphasise that the bolometric luminosity during this transition does not change ($L_{\rm bol} \approx 8 \times 10^{36}\ \rm erg\,s^{-1}$ see Fig. 3, top panel). The most prominent changes are in the parameters of the accretion disc. In the transition, the disc component becomes more luminous, the inner disc temperature $T_{\rm disc}$ increases and the inner disc radius $R_{\rm disc}$ decreases. Before the transition, the bolometric disc luminosity was $L_{\rm disc} \approx 2.4 \times 10^{36}\ \rm erg\,s^{-1}$ and after the transition it increased to $L_{\rm disc} \approx 3.2 \times 10^{36}\ \rm erg\,s^{-1}$. This means that the luminosity of the accretion disc changed from roughly 30 to 40 per cent of the bolometric luminosity, whereas the luminosity of the hotspot decreased. We also detect a significant increase of the hotspot temperature (and the seed photon temperature) and a decrease in the apparent radius of the hotspot. We also note that we do not see any change in the optical depth of the shock as $\tau \approx 1$ throughout the outburst (see Table 2). This suggests that although the characteristic temperatures and radii change in the transition, the properties in the Comptonized emission above ~ 10 keV remain constant. We make use of this result in Section 4.2, where we analyse the simultaneous pulse profile transition.

The spectral fitting indicates that $R_{\rm disc}$ decreases from ≈50 to ≈30 km in the transition, while the inner disc temperature $T_{\rm disc}$ increases from ≈0.3 to ≈0.4 keV. This effect is seen in both *Swift* and *RXTE*/PCA spectra, which is illustrated in Figures 2, 3 and 4. Interestingly, after the transition we see that $R_{\rm disc} \approx R_{\rm co}$, as the co-rotation radius

$$R_{\rm co} = (GM_*/\omega_*^2)^{1/3} \qquad (2)$$

of SAX J1808.4–3658 is about 31 km for a NS mass of $M_* = 1.4\rm M_\odot$ (ω_* is the angular spin frequency of the NS). There is of course an inherent uncertainty in deriving $R_{\rm disc}$ as its value depends on the assumed distance and the inclination as $R_{\rm disc} \propto D/\sqrt{\cos i}$. However, the distance is known rather accurately (Galloway & Cumming 2006) and we will show in Section 4.2 that our initial assumption of $i = 60^\circ$ is consistent with the pulse profile modelling. Other complications in relating modelled radii (both $R_{\rm disc}$ and $R_{\rm bb}$) to "physical" radii are related to the deviation of the local spectra from the blackbody, assumed boundary conditions and relativistic effects. Because these effects do not change the interpretation of the results qualitatively – in the sense that there is only a systematic shift in the modelled radii – we defer the discussion of these effects to Section 5.3.

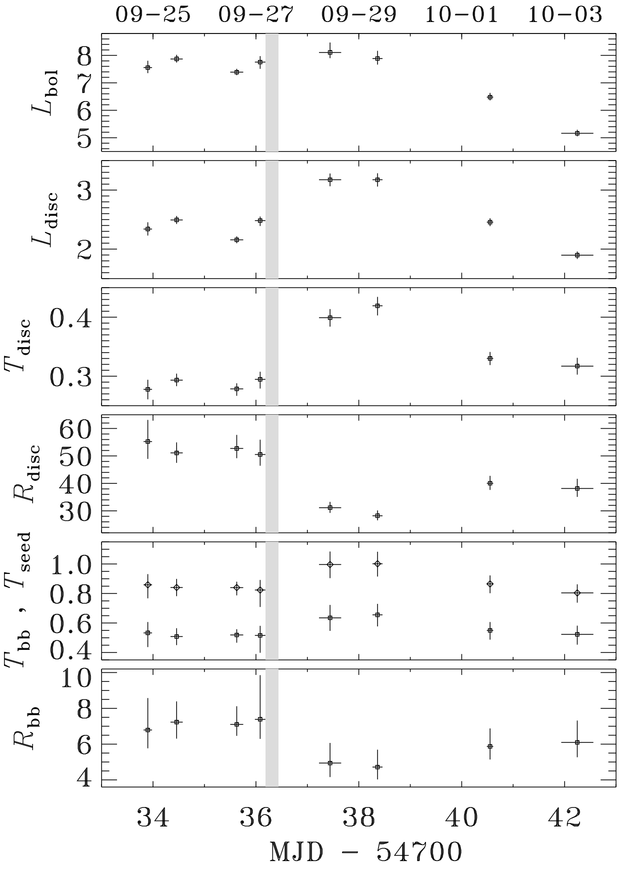

Figure 3. Time evolution of the spectral parameters. Luminosities are given in units of $10^{36}\ \rm erg\,s^{-1}$, temperatures in keV and radii in km. The error bars in time axis denote the time between *Swift* and *RXTE* pointings. The grey area denotes the time period when the spectral and timing transition must have occurred (see the text and Fig. 2). The spectral transition stands out as an increase of the inner disc temperature $T_{\rm disc}$, a decrease of $R_{\rm disc}$ and a change in the hotspot radius and temperature. The bolometric luminosity remains roughly constant at $L_{\rm bol} \approx 8 \times 10^{36}\ \rm erg\,s^{-1}$, which indicates a constant mass accretion rate $\dot{M}$ through the transition. Note also that the values of $R_{\rm disc}$ and $R_{\rm bb}$ are affected by systematic uncertainties, see text.

Table 2. Best-fitting parameters. The fixed parameters were: $N_{\rm H} = 1.13 \times 10^{21}\ {\rm cm}^{-2}$, $T_{\rm e} = 50$ keV, $i = 60°$.

#[a]	$T_{\rm disc}$ (keV)	$K_{\rm disc}$ (km/10 kpc)^2	$T_{\rm bb}$ (keV)	$K_{\rm Fe}$ $[\times 10^{-3}]$	$T_{\rm seed}$ (keV)	τ	$\Re$	$K_{\rm bb}$=$K_{\rm seed}$ (km/10 kpc)^2	$F_{\rm disc}$[b]	$F_{\rm bol}$[b]	$\chi^2_{\rm red}$/d.o.f.
1, 3	$0.28^{+0.02}_{-0.02}$	1250^{+380}_{-270}	$0.53^{+0.07}_{-0.10}$	$1.50^{+0.36}_{-0.35}$	$0.86^{+0.07}_{-0.09}$	$1.05^{+0.11}_{-0.08}$	< 0.40	380^{+220}_{-110}	$1.60^{+0.08}_{-0.07}$	$5.15^{+0.17}_{-0.14}$	1.07/ 371
5, 6	$0.29^{+0.01}_{-0.01}$	1070^{+170}_{-140}	$0.51^{+0.06}_{-0.06}$	$1.50^{+0.25}_{-0.25}$	$0.84^{+0.06}_{-0.06}$	$1.05^{+0.06}_{-0.05}$	$0.21^{+0.11}_{-0.12}$	430^{+150}_{-100}	$1.70^{+0.05}_{-0.05}$	$5.37^{+0.10}_{-0.09}$	1.21/ 550[c]
8, 9	$0.28^{+0.01}_{-0.01}$	1130^{+220}_{-150}	$0.52^{+0.04}_{-0.05}$	$1.55^{+0.23}_{-0.22}$	$0.84^{+0.04}_{-0.05}$	$1.05^{+0.05}_{-0.05}$	$0.21^{+0.11}_{-0.10}$	410^{+130}_{-70}	$1.47^{+0.04}_{-0.04}$	$5.04^{+0.08}_{-0.08}$	1.07/ 545
10, 11	$0.29^{+0.01}_{-0.02}$	1040^{+230}_{-160}	$0.52^{+0.07}_{-0.12}$	$1.62^{+0.44}_{-0.43}$	$0.82^{+0.07}_{-0.11}$	$1.09^{+0.08}_{-0.11}$	< 0.34	450^{+350}_{-120}	$1.69^{+0.05}_{-0.06}$	$5.29^{+0.15}_{-0.17}$	1.22/ 553[c]
13, 14	$0.40^{+0.01}_{-0.02}$	400^{+60}_{-50}	$0.64^{+0.09}_{-0.09}$	$1.51^{+0.46}_{-0.45}$	$1.00^{+0.09}_{-0.09}$	$1.05^{+0.08}_{-0.08}$	< 0.42	200^{+100}_{-60}	$2.17^{+0.07}_{-0.08}$	$5.53^{+0.25}_{-0.14}$	1.01/ 535
16, 17	$0.42^{+0.02}_{-0.02}$	320^{+50}_{-40}	$0.66^{+0.07}_{-0.08}$	$1.59^{+0.40}_{-0.40}$	$1.00^{+0.08}_{-0.09}$	$1.09^{+0.12}_{-0.09}$	< 0.35	180^{+80}_{-50}	$2.17^{+0.08}_{-0.08}$	$5.38^{+0.19}_{-0.15}$	1.08/ 533
21, 22	$0.33^{+0.01}_{-0.01}$	650^{+90}_{-80}	$0.55^{+0.06}_{-0.06}$	$1.44^{+0.22}_{-0.22}$	$0.87^{+0.06}_{-0.06}$	$1.02^{+0.08}_{-0.06}$	$0.27^{+0.16}_{-0.16}$	280^{+110}_{-70}	$1.68^{+0.05}_{-0.05}$	$4.42^{+0.10}_{-0.08}$	1.11/ 533
24, 25	$0.32^{+0.01}_{-0.01}$	590^{+110}_{-90}	$0.52^{+0.06}_{-0.07}$	$1.30^{+0.18}_{-0.18}$	$0.80^{+0.06}_{-0.07}$	$0.98^{+0.10}_{-0.08}$	$0.38^{+0.23}_{-0.21}$	300^{+130}_{-80}	$1.29^{+0.04}_{-0.04}$	$3.52^{+0.09}_{-0.07}$	1.02/ 484

[a] Observation numbers from Table 1. [b] Flux in units of $10^{-9}\ {\rm erg\,cm^{-2}\,s^{-1}}$. [c] Poor fits are mainly due to large residuals in XRT spectra around ≈ 2 keV, which are most likely due to a calibration issue at the Si Kα edge at 1.839 keV (Godet et al. 2009). Removing the data between 1.6–2.4 keV improves the fits to $\chi^2_{\rm red} \approx 1.1$, without a significant change in the best-fitting parameters.

In accretion on to neutron stars one expects that a constant fraction of the available accretion power is released in photon luminosity; what is not radiated in the disc, will be radiated at the NS surface. Therefore, the observed luminosity is thought to be a good measure of the mass accretion rate $\dot{M}$. As the bolometric luminosity during this transition does not change, we can conclude that the sudden change in the disc parameters cannot be caused by a sudden increase in the mass accretion rate. This points towards the conclusions that the change in $R_{\rm disc}$ is not related to a change in the truncation radius (which is proportional to the Alfvén radius, where the pressure of the NS magnetic field equals the ram pressure of the accreting gas, e.g. Long et al. 2005)

$$R_{\rm t} = k_{\rm A}(2GM_*)^{-1/7}\dot{M}^{-2/7}\mu^{4/7}. \tag{3}$$

Here $\mu = B_{\rm S}R_*^3$ is the NS magnetic moment and R_* is the NS radius. The truncation radius $R_{\rm t}$ is also commonly called the magnetospheric radius, but in the following we instead use this term to define the outermost radius $R_{\rm m}$ where the field lines of the NS are coupled with the accretion disc (Lovelace et al. 1995, hereafter LRB95). We propose that the interaction region between the disc and the NS magnetic field is large (so that $R_{\rm m} > R_{\rm t}$, see Fig. 4, bottom panels) and that the modelled inner disc radius actually corresponds to the magnetospheric radius $R_{\rm disc} \sim R_{\rm m}$ and not the truncation radius $R_{\rm t}$.

4 VARYING DISC–MAGNETOSPHERE COUPLING IN SAX J1808.4–3658

4.1 Physical picture

We interpret the spectral transition to be caused by a change in the way the dipole field of the NS is coupled with the accretion disc. The reason for the observed spectral and timing transition is most likely caused by opening of the field lines.

Many theoretical studies of the disc–magnetosphere coupling have been published (e.g. Ghosh & Lamb 1979a,b; Wang 1987; Lovelace et al. 1995; Rappaport et al. 2004; Kluźniak & Rappaport 2007). Here we use the framework developed by LRB95 to interpret the observed transition (see Uzdensky 2004, for a review of alternative models). In the LRB95 model, the magnetic field configuration is such that close to the accreting NS the field lines are closed (defined here as the magnetosphere) and outside the magnetosphere the field lines are open (see Fig. 4). The field lines decouple from the disc because of a large difference in the angular velocity of the Keplerian disc and the NS (except at $R_{\rm co}$). As the disc is a good conductor, the NS magnetic field is "frozen" into it and the twisting of the field lines caused by the differential rotation creates a toroidal field component B_ϕ out of the poloidal field B_z. However, there is a critical twist of $\gamma_{\rm c} = B_\phi/B_z \sim 1$ after which the increased magnetic pressure tends to open the field lines, thus severing the link between the NS and the disc (see LRB95, Uzdensky et al. 2002a,b; Uzdensky 2004 and references therein).

Within the magnetosphere ($r < R_{\rm m}$), the magnetic field threading the disc can force the gas to co-rotate with the NS so that $\omega(r) \approx \omega_*$ (LRB95), which is also seen in MHD simulations (e.g. Romanova et al. 2002). This has a strong effect on the radiation flux emitted from the disc, which is most easily seen from the energy conservation equation (see eq. 7 in LRB95)

$$\Sigma\nu_{\rm t}\left(r\frac{{\rm d}\omega}{{\rm d}r}\right)^2 + \frac{4\pi}{c^2}\int_{-H}^{H}{\rm d}z\,\eta_{\rm t}\boldsymbol{J}^2 \equiv 2\sigma_{\rm SB}T_{\rm eff}^4. \tag{4}$$

Here Σ is the surface density, $\nu_{\rm t}$ is the turbulent viscosity (which is assumed to be described by the alpha prescription $\nu_{\rm t} = \alpha c_{\rm s}H$, Shakura & Sunyaev 1973), $c_{\rm s}$ is the sound speed, z is the coordinate along the normal to the disc plane, H is the disc height, $\eta_{\rm t}$ is the magnetic diffusivity of the disc, $\boldsymbol{J}$ is the current density, $\sigma_{\rm SB}$ is the Stefan-Boltzmann constant and $T_{\rm eff}$ is the effective temperature of the disc. In equation (4) the first term in the left hand side is the viscous dissipation rate per unit area, the second term is the Ohmic dissipation rate and the right hand side is the flux radiated by the optically thick and geometrically thin disc. If $\omega(r) \approx \omega_*$ within the magnetosphere ($r < R_{\rm m}$), the viscous dissipation $\propto ({\rm d}\omega/{\rm d}r)^2$ is strongly suppressed and the Ohmic dissipation becomes the dominant energy release mechanism (LRB95). Expressing the current density through the accretion velocity v_r and vertical magnetic field strength $B_z = B_{\rm S}(R_*/r)^3$ as $J = (c^2/4\pi\eta_{\rm t})(v_r/c)B_z$ and integrating equation (4) over the radius we get an order of magnitude estimate of the luminosity due to the Ohmic dissipation (see also Wang et al. 1990):

$$L_{\rm Ohm} \sim \frac{H}{\eta_{\rm t}}\int_{R_{\rm t}}^{R_{\rm m}} v_r^2 B_z^2 r{\rm d}r \sim \frac{Hv_r^2}{\eta_{\rm t}}B_{\rm S}^2R_*^2\frac{R_*}{R_{\rm t}}. \tag{5}$$

For geometrically thin disc $H/r \sim 0.01$ with $c_{\rm s} \lesssim 10^8$ cm s^{-1}, substituting $v_r \sim \alpha c_{\rm s}H/r$ (e.g. Frank et al. 2002), $\eta_{\rm t} \sim \nu_{\rm t} = \alpha c_{\rm s}H$ (Fromang & Stone 2009) and $\alpha < 1$, we can show that $L_{\rm Ohm} \ll 10^{35}\ {\rm erg\,s^{-1}}$ for the typical parameters of SAX J1808.4–

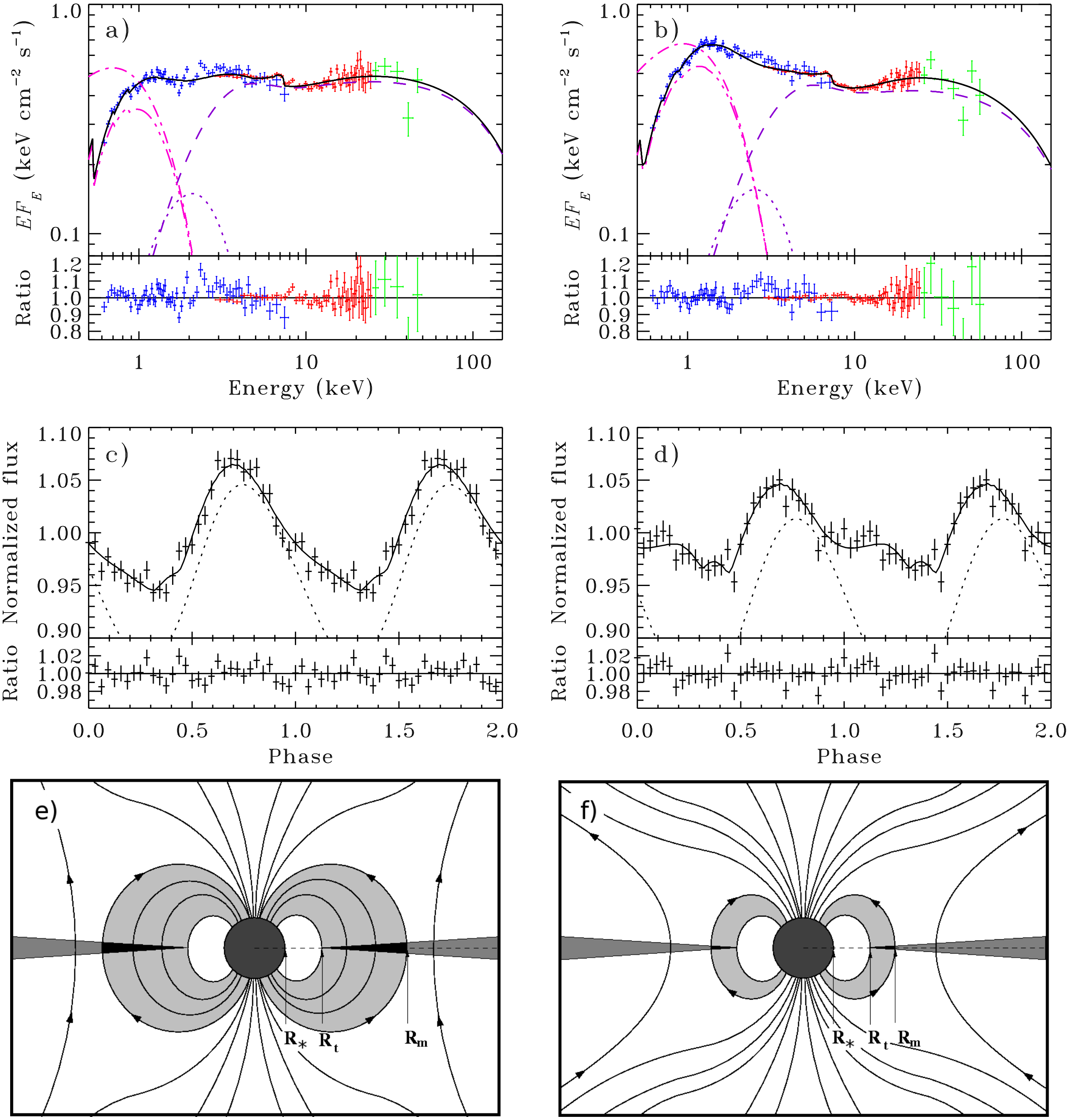

Figure 4. Photon spectra before the transition (from observations 10 and 11, see Table 1) and after the transition (from observations 13 and 14) are shown in the top panels (a) and (b), respectively. The blue, red and green data points are for *Swift*/XRT, *RXTE*/PCA and *RXTE*/HEXTE, respectively. The solid black line shows the model spectrum. The pink dot-dashed line is the unabsorbed disc component and the three-dot-dashed line the absorbed disc component. The purple dotted line is the NS blackbody component, whereas the dashed line is the Comptonized component. The weak Compton reflection and the iron line are below the plotting range so that the spectral transition is more easily visualized. Pulse profile before the transition (from observations 9 and 10) and after the transition (from observation 12) are shown in the middle panels (c) and (d), respectively. The solid line is the contribution from both spots, whereas the dotted line shows the contribution of the "main" spot. Lower panels illustrate the geometry of the disc–magnetosphere interaction region before (panel e) and after (panel f) the transition. The dark region in the accretion disc within $R_{\rm t} < r < R_{\rm m}$ is assumed to rotate as $\omega(r) \approx \omega_*$ so that the energy dissipation rate in that region is strongly suppressed.

3658 ($B_{\rm S} \sim 10^8$ G, $R_* \approx 10$ km, $R_{\rm t} \approx 20$ km).[1] Thus the Ohmic dissipation within the magnetosphere is much smaller than the viscous dissipation outside the magnetosphere ($r > R_{\rm m}$), and therefore does not contribute much to the observed flux from the disc. Therefore, the inner disc radius $R_{\rm disc}$ derived from the spectral fits actually should correspond to the magnetospheric radius $R_{\rm m}$. This makes the physical interpretation of the transition rather straightforward.

If $R_{\rm disc} \sim R_{\rm m}$, the reconfiguration during the transition can be understood as opening of the field lines (see Fig. 4, bottom panels). Initially the interaction region between the magnetosphere and the disc is large, such that it extends from the truncation radius $R_{\rm t} \approx 20$ km to $R_{\rm m} \sim 50$ km. Then the field lines open resulting in a smaller $R_{\rm m} \sim 30$ km, so that the region of the suppressed dissipation (where $\omega \approx \omega_*$) is smaller (dark regions in the disc in the bottom panels of Fig. 4). This readily explains why there is an increase in the inner disc temperature $T_{\rm disc}$, a decrease of $R_{\rm disc}$ and why $L_{\rm disc}/L_{\rm bol}$ increases.

The fitting indicates that $R_{\rm m} \gtrsim R_{\rm co}$ before the transition, but we note that the exact value of $R_{\rm m}$ is rather uncertain (see Section 5.3). According to Rappaport et al. (2004) $R_{\rm m}$ can exceed the corotation radius by 30 per cent before the centrifugal barrier halts the accretion. This might set the upper limit for $R_{\rm m}$ before the transition. Then, the sudden opening of the field lines (decrease of $R_{\rm m}$) could be caused by a change in the properties of the accretion disc. In the LRB95 model $R_{\rm m}$ is determined by the critical twist $\gamma_{\rm c} = B_\phi/B_z = -Hr(\omega(r) - \omega_*)/\eta_{\rm t}$. As $\gamma_{\rm c} \approx 1$ (e.g. Uzdensky et al. 2002a,b) is thought to be a constant, a change in the magnetospheric radius $R_{\rm m}$ – for a fixed $\dot{M}$ – could be caused by a change in the magnetic diffusivity $\eta_{\rm t}$. Furthermore, as the diffusivity $\eta_{\rm t}$ is most likely caused by the same MHD turbulence that produces the viscosity $\nu_{\rm t}$ (so that $\eta_{\rm t} \sim \nu_{\rm t}$, Fromang & Stone 2009) we speculate that the observed spectral- and timing transition could be related to changes of viscosity in the accretion disc. Also, recent MHD simulations have shown that if the magnetic Reynolds number ($= c_{\rm s}H/\eta_{\rm t}$) is below a certain critical value, the magneto-rotational instability (Balbus & Hawley 1998) that is believed to be responsible for the angular momentum transport in the accretion disc might quench, possibly causing high- and low viscosity states (Simon et al. 2011). If the pulse profile variability – and in general the timing noise – in AMPs is ultimately caused by such a mechanism, observations of AMPs could be used to place constraints for $\eta_{\rm t}$ and $\nu_{\rm t}$ because for many AMPs the key parameters such as $B_{\rm S}$, $\dot{M}$ and the relevant radii and temperatures are rather accurately known.

4.2 Pulse profile modelling

The observed spectral transition can be caused by a change in the coupling between the magnetic field of the NS and the accretion disc. Changes in the geometry of the disc–magnetosphere interaction region, on the other hand, alter the way the accretion flow gets channelled onto the NS surface and cause variations in the hotspot size and shape, which affect the pulse profiles (see Fig. 4). MHD simulations of Romanova et al. (2004) showed that the spot shape strongly depends on the magnetic inclination θ, the angle between the magnetic pole and the rotational axis. For $\theta \lesssim 15^\circ$ – which is most likely the case for SAX J1808.4–3658 (e.g. Ibragimov & Poutanen 2009) – the spot shape is close to a ring.

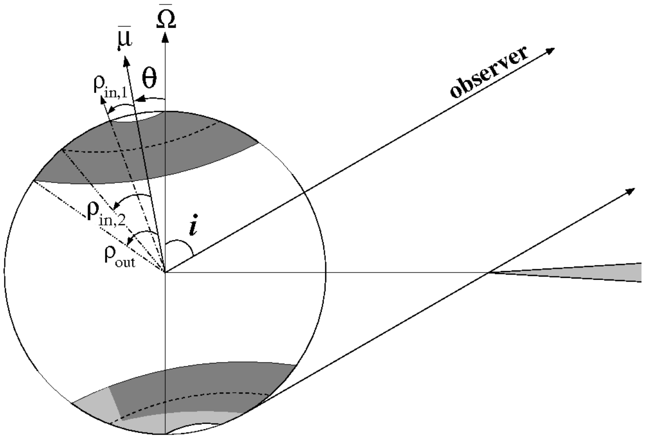

Figure 5. Geometry of the hotspots. The magnetic dipole is inclined by angle θ to the spin axis and the co-aligned hotspots are assumed to be ring-shaped. The inner edges of the hotspots are displaced from the magnetic poles by angle $\rho_{\rm in}$ and the outer edges by $\rho_{\rm out}$. The accretion disc truncation radius, that determines which part of the secondary hotspot is blocked, is related to $\rho_{\rm out}$ using equation (6). The pulse profile variations can be modelled simply by changing $\rho_{\rm in}$ (which is a function of $R_{\rm m}$) as shown in Section 4.2.

We thus assume that the hotspot shape is a ring around the magnetic pole so that the size of the hotspot is determined by the inner hotspot edge $\rho_{\rm in}$ and the outer hotspot edge $\rho_{\rm out}$ (see Fig. 5). By further assuming that the NS magnetic field is a dipole, $\rho_{\rm in}$ and $\rho_{\rm out}$ can be related to the magnetospheric radius and the disc truncation radius (see e.g. Frank et al. 2002; Poutanen et al. 2009):

$$\sin\rho_{\rm in} = \cos\theta\sqrt{R_*/R_{\rm m}}, \quad \sin\rho_{\rm out} = \cos\theta\sqrt{R_*/R_{\rm t}}. \qquad (6)$$

We also assume that changes in the magnetosphere size do not affect the truncation radius $R_{\rm t}$. This can be justified as the detailed mechanism of the interaction should not play a big role owing to the strong ($\propto r^{-6}$) radial dependence of the magnetic energy density, which – for a given $\dot{M}$ – determines the location of $R_{\rm t}$. Obviously parameters such as M_*, R_*, i, θ and $B_{\rm S}$ do not change in the transition either. What is expected, however, is that the hotspot size should change, which was also seen in the modelling of the time averaged spectra in section 3.3. This can be seen as a natural consequence of the opening of the field lines. As illustrated in Fig. 4, the field lines that connect the disc at $R_{\rm m}$ are the ones that connect closest to the magnetic pole of the NS. Given our assumption that $R_{\rm t}$ is constant, $\rho_{\rm out}$ is also constant as θ is constant. Therefore, under these assumptions, the change in the hotspot size can only be caused by a change of the inner hotspot edge $\rho_{\rm in}$ (see Figs 4 and 5). Furthermore, the opening of the field lines would not change the hotspot centroid, and thus would not cause a jump in the pulse phases. As we do not see any such change in phases immediately after the pulse profile change (see Fig. 1), our choice of a hotspot as a symmetric ring around the magnetic pole seems to approximate the emission region to a sufficient accuracy.

We use the PCA data from observations 9 and 10 for the "pre-transition" pulse profile and observation 12 for the "after-transition" pulse profile. We only concentrate on the pulse profile changes in the hard band (9.8–23.2 keV) for two reasons. (1) In the hard band we have emission only from the Comptonized component, whereas in the soft band blackbody component also contributes. (2) In the hard band we have emission from high scattering orders (Viironen & Poutanen 2004; Poutanen 2008), where the energy and angular distributions of the radiation intensity $I(E, \zeta)$ at the stellar surface can be approximated with a simple formula:

---

[1] We constrain the truncation radius to $R_{\rm t} \approx 20$ km from the pulse profile modelling in Section 4.2.

$$I(E, \zeta) \propto (1 - h\cos\zeta)E^{-(\Gamma-1)}, \qquad (7)$$

where E is the photon energy, ζ is the angle relative to the surface normal, h is the anisotropy parameter and Γ is the power-law photon index ($\Gamma \approx 2$ for SAX J1808.4–3658).

We fitted the profiles with the model described in detail in Poutanen & Gierliński (2003) and Poutanen & Beloborodov (2006). The model accounts for special relativistic effects (such as Doppler boosting and aberration) as well as the general relativistic effects (redshift and light bending). We also account for the eclipses of the hotspot by the accretion disc as described by Ibragimov & Poutanen (2009). We initially arbitrarily chose $M_* = 1.4\mathrm{M}_\odot$, $R_* = 10.3$ km, $i = 60^\circ$. We set θ and ρ_out as free parameters, but forced them to be the same for the two pulse profiles. R_t was computed from ρ_out and θ using equation (6). An additional free parameter is the phase shift ϕ_shift describing the displacement of the pulse peak. Because the extracted pulse profiles were separated by one day and no shifts in phases were seen (see Fig. 1), we force ϕ_shift to be the same for both pulse profiles. The only parameters that we initially let to vary in the transition were ρ_in and h, which in our view could change if the disc–magnetosphere coupling changes.

However, the strong secondary pulse after the transition (which we associate with the secondary spot) proved to be problematic to model. The only way we could get such a peculiar shape was that the secondary spot was partially blocked by the accretion disc (we assume that the secondary spot is antipodal). We realised that the reason we did not get a good fit to the data was our guess of M_*, R_* and i. We then let R_* and i to vary in the fitting and found that there was a rather tight range of these parameters that we could produce such a pulse shape. We found that for $M_* = 1.4\mathrm{M}_\odot$, only with a NS radius of $R_* \approx 11$ km were we able to produce the pulse shape correctly. Furthermore, in the initial fitting we did not see a significant change in the h parameter between the two pulses as it varied in a tight range of $h \approx 0.57 \pm 0.05$. This is actually expected since h fundamentally depends on the optical depth τ (Poutanen 2008), which did not change in the transition (see Fig. 3 and Table 2). Values of $h \gtrsim 0.5$ correspond to optically thin shocks (Poutanen 2008), so the values of $\tau \approx 1$ and $h \approx 0.57$, obtained here independently from spectral and pulse profile modelling are consistent with each other. Therefore, we let h to be free parameter, but required it to be the same for both pulses.

Thus, the modelling was performed with parameters h, ρ_out, i, θ and ϕ_shift and the parameters that were allowed to vary between the pulses were $\rho_\mathrm{in,1}$ and $\rho_\mathrm{in,2}$. The best-fitting parameters of the modelling are presented in Table 3. The corresponding pulse profiles are shown in Figs 4(c) and (d), where the dashed line shows the contribution of the main hotspot, and the solid line shows the sum of the main and the secondary hotspots. The results indicate that the secondary hotspot is almost entirely blocked (by the NS itself and the accretion disc) around phase 0, and becomes partially visible around phase 0.5. The overall contribution of the secondary hotspot to the observed flux increases in the transition from about 5 to 10 per cent mostly because of the increase of the hotspot temperature (associated with the decreasing size). We also see that for the assumed $M_* = 1.4\mathrm{M}_\odot$ and $R_* = 11$ km, we get physically plausible results for all the free parameters.

(i) The inclination is roughly $i \approx 60^\circ$, which is consistent with previous estimations (Deloye et al. 2008; Ibragimov & Poutanen 2009).

(ii) The value of the anisotropy parameter $h \approx 0.57$ is also what we expect from Comptonization of optical depth $\tau \approx 1$ (Poutanen 2008), that was seen in the time averaged spectra.

(iii) The magnetic inclination $\theta \approx 10^\circ$ is consistent with the assumption that the shape of the hotspots are close to a ring (Romanova et al. 2004) and similar to previous constraints (Ibragimov & Poutanen 2009).

(iv) The truncation radius $R_\mathrm{t} \approx 20$ km, which is within the co-rotation radius of $R_\mathrm{co} = 31$ km and is smaller than $R_\mathrm{m} \approx R_\mathrm{co}$, which is what we expected.

(v) Most importantly, the increase of ρ_in from $< 12^\circ$ to $\approx 30^\circ$ is what is expected, if the transition in the spectrum and the pulse profile are both caused by a decrease of R_m. Therefore, we see that the results of the pulse profile modelling are consistent with our interpretation and – taken together with the spectral information – fully support the picture that the pulse profile changes in SAX J1808.4–3658 are a consequence of a dynamic magnetosphere.

Table 3. Best-fitting parameters from the pulse profile modelling.

Parameter	Value	Units
NS mass M_*	1.4 (fixed)	$\mathrm{M}_\odot$
NS radius R_*	11 (fixed)	km
Inclination i	58^{+4}_{-6}	deg
Magnetic inclination θ	11 ± 1	deg
Outer spot radius ρ_out	46 ± 6	deg
Inner spot radius before transition $\rho_\mathrm{in,1}$	<12	deg
Inner spot radius after transition $\rho_\mathrm{in,2}$	31 ± 2	deg
Disc truncation radius R_t ^{a}	21^{+5}_{-3}	km
Anisotropy parameter h	0.57 ± 0.03	
χ^2/d.o.f.	62.7/57	

^{a} R_t is not a free parameter, it was computed using Eq. (6).

5 DISCUSSION

5.1 Implications for spin-up torques during the outburst

The changes in the interaction between the disc and the magnetosphere can have a large effect on the torque that spins up (or spins down) the NS. Several different models have been developed to compute the torques (e.g. Ghosh & Lamb 1979a,b; Wang 1987; Lovelace et al. 1995; Rappaport et al. 2004; Matt & Pudritz 2005; Kluźniak & Rappaport 2007; Matt et al. 2010). Generally, in addition to the "accretion torque" $\tau_\mathrm{a} = \dot{M}\sqrt{GM_* R_\mathrm{t}}$ (e.g. Matt et al. 2010), the disc–magnetosphere coupling can cause an additional "magnetic torque," which is strongly dependent on the nature of the interaction and varies significantly between the models. Nevertheless, it can be concluded that small variations of R_m independent of the mass accretion rate (as observed here for SAX J1808.4–3658) can cause the NS spin-up or spin-down depending on the geometry and position of R_m relative to R_co.

Also the data suggests, that only those models that predict that $\omega \approx \omega_*$ in the magnetosphere can be valid to explain the observed spectral transition. So observations of AMPs – as presented here – can be used to test different hypothesis and constrain the nature of the disc–magnetosphere coupling.

5.2 Implications for the timing noise in AMPs

Although the pulse amplitude dropped significantly, the pulse phase remained constant during the transition. This is actually not surprising, based on the fact that the magnetic inclination seems to be about $\theta \approx 10^{\circ}$. As the hotspot shape is most likely close to a ring (Romanova et al. 2004), the change in $R_{\rm m}$ should only affect the location of the inner edge of the hotspot $\rho_{\rm in}$, but not change the location of the hotspot on the NS surface. However, the situation might be different for other AMPs, where θ can be larger. For such AMPs, the hotspot shapes are most certainly not symmetric (Romanova et al. 2004), and changes in $R_{\rm m}$ might result in a change in the shape, size, latitude and –most importantly– the hotspot longitude. Shifts in the hotspot longitude can especially cause large jumps in the observed pulse phases (see Lamb et al. 2009, for discussion). We speculate that such $R_{\rm m}$–dependent motion of the hotspots (and the associated phase jumps) could be the origin of at least part of the timing noise in AMPs. Observationally, such mechanism could cause the outliers in the X-ray flux – phase residual relations in XTE J1807–294 (Riggio et al. 2008; Patruno et al. 2009c, 2010b), XTE J0929–314 (Galloway et al. 2002; Patruno et al. 2009c) and IGR J17511–3057 (Riggio et al. 2011; Ibragimov et al. 2011), whereas the overall X-ray flux – phase residual trends can be caused by $\dot{M}$–dependent motion of the hotspots (Lamb et al. 2009; Patruno et al. 2009c, 2010b). Also, we stress that an additional contribution to the timing noise can be caused by $\dot{M}$–dependent variation of the truncation radius $R_{\rm t}$, as it affects the visibility of the secondary spot (Ibragimov & Poutanen 2009; Poutanen et al. 2009). These factors do not however exclude the possibility that some AMPs do spin-up during X-ray outbursts (as is most likely the case with IGR J00291+5934, e.g. Falanga et al. 2005; Burderi et al. 2007; Patruno 2010b; Hartman et al. 2011; Papitto et al. 2011).

5.3 Possible caveats

(i) The truncation radius of $R_{\rm t} \approx 20$ km was obtained from pulse profile modelling. We assumed that this radius is not affected by the change in the disc–magnetosphere coupling that we propose to be the reason for the transition. We also assumed that the outer edge of the ring-shaped hotspot $\rho_{\rm out}$ is determined from equation (6), which is not necessarily the case as the field topology should differ from a pure dipole. These factors can change the constraints on the other parameters. However, a detailed analysis of these factors should be done by 3D MHD simulations (as in Romanova et al. 2004), but such a study is clearly beyond the scope of the present paper.

(ii) As the Ohmic dissipation in the magnetosphere is small, we proposed that $R_{\rm disc} \sim R_{\rm m}$. However, there are some uncertainties in deriving $R_{\rm disc}$ in addition to those related to spectral modelling in Section 3.2. The main systematic uncertainty in estimating $R_{\rm m}$ from $R_{\rm disc}$ comes from the fact that $T_{\rm disc}$ is in reality a colour temperature and not the effective temperature of the disc. Also, the inner disc boundary condition might differ significantly from what is assumed in the DISKBB model, where the radial dependence of temperature is $T(r) \propto r^{-3/4}$. These effects could be, in principle, accounted for to obtain the corrected inner disc radius

$$R'_{\rm disc} = \xi f_{\rm col}^2 R_{\rm disc}, \qquad (8)$$

where ξ accounts for the fact that the modelled inner disc temperature $T_{\rm disc}$ does not actually occur at $R_{\rm disc}$ and $f_{\rm col}$ is the colour correction factor (Gierliński et al. 1999). The colour correction factor was computed to be $f_{\rm col} \approx 1.7$ by Shimura & Takahara (1995) for black hole systems in the soft state and it seems to be weakly dependent of the mass accretion rate (see Davis et al. 2005). The correction factor $\xi = 0.37$ was computed by Gierliński et al. (1999) by assuming a zero torque boundary condition at the inner edge of the disc in the pseudo-Newtonian potential. However, because of the different inner disc boundary conditions for accretion onto an AMP ξ can be much different especially in the beginning of the outburst, where the spectral modelling indicates that $R_{\rm m} \gtrsim R_{\rm co}$ and therefore $\omega_{\rm K} < \omega_*$. In this case, there should be a region around $R_{\rm m}$ where a large jump from the Keplerian rotation to the co-rotation should occur (LRB95, Lovelace et al. 2010). An estimate of the size of this “transition region” Δr was given by LRB95

$$\Delta r \sim \gamma_{\rm c} \frac{\eta_{\rm t} c_{\rm s}}{\omega_{\rm K} \nu_{\rm t}}. \qquad (9)$$

For a thin accretion disc $c_{\rm s}/v_{\rm K} \sim H/r \ll 1$, so at $r = R_{\rm m}$ the transition region $\Delta r \sim H \ll R_{\rm m}$ assuming that $\eta_{\rm t} \sim \nu_{\rm t}$ and $\gamma_{\rm c} \sim 1$. Therefore, we speculate that its effect on the observed radiation flux is small due to the small size, but the exact value of the correction factor ξ is uncertain. Furthermore, as the accretion disc is irradiated by the emission of the hotspot and part of the hard emission is absorbed by the disc, the observed colour temperature can be altered and therefore affect $R_{\rm disc}$. But because the amplitude of Compton reflection $\Re$ is poorly constrained, it is not possible to accurately take this effect into account. All these unknown factors cause a systematic error in $R_{\rm disc}$, which makes an accurate estimation of $R_{\rm m}$ currently infeasible.

Similarly, the hotspot temperature $T_{\rm bb}$ is also a colour temperature (at the infinity), but $f_{\rm col}$ is most likely the order of unity in this case (see Gierliński & Poutanen 2005, and references therein) and the actual hotspot size can be larger depending on the stellar compactness and the hotspot geometry (e.g. Poutanen & Gierliński 2003; Gierliński & Poutanen 2005; Ibragimov & Poutanen 2009). These considerations only change the reported results quantitatively, but the qualitative result of the hotspot size variation shown in Fig. 3 is not affected.

(iii) In our modelling we did not consider any complicated spot shapes. Based on the simulations of Romanova et al. (2004) a crescent shaped spot might have been more appropriate to use. However, this would have required several new parameters to the model, which is not justified based on the quality of the data. This cannot be improved because the pulse profile changes so rapidly that co-adding more data would not be appropriate. Also by selecting a broader range in energies than the 9.8–23.2 keV band to improve the statistics cannot be done easily, because the blackbody component (with a different emission pattern) will start contributing from below and there are not enough photons above this range. Therefore, the only way to address this issue is by making extensive simulations and to extract pulse profiles from all the outbursts of SAX J1808.4–3658 and then simultaneously fit them.

6 SUMMARY

We have studied spectral and pulse profile variability of SAX J1808.4–3658 during its 2008 outburst. We found that the large drop in the pulse amplitude and the associated change of the pulse profile on September 27 (see fig. 1 in Hartman et al. 2009) was accompanied by a simultaneous spectral transition in the accretion disc, which was most evidently seen in the *Swift* data. Our interpretation of this transition is that the magnetospheric radius $R_{\rm m}$ changes because of opening of the field lines that connect the NS magnetic field to the accretion disc. We speculated that the physical origin of the field line opening is related to the change of magnetic diffusivity $\eta_{\rm t}$ or viscosity $\nu_{\rm t}$. Through this interpretation we could explain why the apparent inner disc radius – which we associate with the magnetospheric radius $R_{\rm m} \sim R_{\rm disc}$ – decreases from 50 to 30 km in the spectral modelling, why the accretion disc temperature increases from 0.3 to 0.4 keV and why the disc contribution to the bolometric flux increases from 30 to 40 per cent.

We also saw a decrease in the apparent radius of the hotspot in the spectral analysis and this is also consistent with our interpretation. The field lines that connect the disc at $R_{\rm m}$ are the ones that connect closest to the magnetic pole of the NS. As we assumed that the hotspot shape is a ring around the magnetic pole, the opening of the field lines should change the location of the inner hotspot edge $\rho_{\rm in}$. Therefore, as the outer hotspot edge $\rho_{\rm out}$ should not change in the transition – because for a dipole magnetic field its mostly determined by the mass accretion rate that remained constant – we can associate the decrease in the hotspot radius to a change in the value of $\rho_{\rm in}$. Our pulse profile modelling showed that this is exactly what is required to produce the observed transition. Furthermore, our results from the pulse profile modelling for the other unknown parameters, such as θ and i, were also consistent with previous estimates. We did not try to place constrains on the neutron star mass and radius based on these data, but the identification that varying hotspot size can lead to pulse profile changes has profound implications for determination of these most important parameters. However, in order to place tight constraints, we should not only concentrate on modelling these two specific pulse profiles, but instead make use of all the outbursts of SAX J1808.4–3658. A detailed re-analysis of these data will the main attention of our future work.

To summarize, for the first time we have found evidence that a sudden pulse profile transition in SAX J1808.4–3658 was most likely caused by a change in the way that the NS magnetic field is coupled to the accretion disc. This mechanism can be one of the causes for pulse profile variability (and the associated timing noise) in other AMPs as well. We constrained the disc truncation radius at $R_{\rm t} = 21^{+5}_{-3}$ km and estimated the magnetospheric radius to be about $R_{\rm m} \sim 30$–50 km. This would allow in principle to estimate the torques acting on the NS, but the spectroscopic determination of $R_{\rm m}$ suffers from several systematic uncertainties that currently prevent such an attempt. This, however, could be improved if radial profiles of ω, B_z and B_ϕ in the magnetospheric region ($R_{\rm t} < r < R_{\rm m}$) were accurately known.

ACKNOWLEDGEMENTS

This work was supported by the Finnish Graduate School in Astronomy and Space Physics (JJEK), EU FP6 Transfer of Knowledge Project "Astrophysics of Neutron Stars" MTKD-CT-2006-042722 (AI), Väisälä foundation (MA), and the Academy of Finland grant 127512 (JP). AP acknowledges partial support from the Netherlands Organization for Scientific Research (NWO) Veni Fellowship and from a ESF/COMPSTAR visit grant. We thank the referee for helpful comments. This research made use of the NASA Astrophysics Data System and of the data obtained from the High Energy Astrophysics Science Archive (HEASARC), which is a service of the Astrophysics Science Division at NASA/GSFC and the High Energy Astrophysics Division of the Smithsonian Astrophysical Observatory.

REFERENCES

Altamirano D., et al. 2011, ApJ, 727, L18

Arnaud K. A., 1996, in Jacoby G. H., Barnes J., eds, ASP Conf. Ser. Vol. 101, Astronomical Data Analysis Software and Systems V. Astron. Soc. Pac., San Francisco, p. 17

Balbus S. A., Hawley J. F., 1998, Reviews of Modern Physics, 70, 1

Bildsten L., Chakrabarty D., 2001, ApJ, 557, 292

Burderi L., Di Salvo T., Menna M. T., Riggio A., Papitto A., 2006, ApJ, 653, L133

Burderi L. et al., 2007, ApJ, 657, 961

Burderi L., Riggio A., di Salvo T., Papitto A., Menna M. T., D'Aì A., Iaria R., 2009, A&A, 496, L17

Cackett E. M., Altamirano D., Patruno A., Miller J. M., Reynolds M., Linares M., Wijnands R., 2009, ApJ, 694, L21

Chakrabarty D., Morgan E. H., 1998, Nat, 394, 346

Davis S. W., Blaes O. M., Hubeny I., Turner N. J., 2005, ApJ, 621, 372

Deloye C. J., Heinke C. O., Taam R. E., Jonker P. G., 2008, MNRAS, 391, 1619

Fabian A. C., Rees M. J., Stella L., White N. E., 1989, MNRAS, 238, 729

Falanga M., et al. 2005, A&A, 444, 15

Frank J., King A., Raine D. J., 2002, Accretion Power in Astrophysics. Cambridge University Press, Cambridge

Fromang S., Stone J. M., 2009, A&A, 507, 19

Galloway D. K., Cumming A., 2006, ApJ, 652, 559

Galloway D. K., Chakrabarty D., Morgan E. H., Remillard R. A., 2002, ApJ, 576, L137

Ghosh P., Lamb F. K., 1979a, ApJ, 232, 259

Ghosh P., Lamb F. K., 1979b, ApJ, 234, 296

Gierliński M., Poutanen J., 2005, MNRAS, 359, 1261

Gierliński M., Done C., Barret D., 2002, MNRAS, 331, 141

Gierliński M., Zdziarski A. A., Poutanen J., Coppi P. S., Ebisawa K., Johnson W. N., 1999, MNRAS, 309, 496

Gilfanov M., Revnivtsev M., Sunyaev R., Churazov E., 1998, A&A, 338, L83

Godet O. et al., 2009, A&A, 494, 775

Hartman J. M. et al., 2008, ApJ, 675, 1468

Hartman J. M., Patruno A., Chakrabarty D., Markwardt C. B., Morgan E. H., van der Klis M., Wijnands R., 2009, ApJ, 702, 1673

Hartman J. M., Galloway D. K., Chakrabarty D., 2011, ApJ, 726, 26

Ibragimov A., Poutanen J., 2009, MNRAS, 400, 492

Ibragimov A., Kajava J. J. E., Poutanen J., 2011, MNRAS, in press [arXiv:1102.1909]

in 't Zand J. J. M., Heise J., Muller J. M., Bazzano A., Cocchi M., Natalucci L., Ubertini P., 1998, A&A, 331, L25

Jahoda K., Markwardt C. B., Radeva Y., Rots A. H., Stark M. J., Swank J. H., Strohmayer T. E., Zhang W., 2006, ApJS, 163, 401

Kluźniak W., Rappaport S., 2007, ApJ, 671, 1990

Lamb F. K., Boutloukos S., Van Wassenhove S., Chamberlain R. T., Lo K. H., Clare A., Yu W., Miller M. C., 2009, ApJ, 706, 417

Long M., Romanova M. M., Lovelace R. V. E., 2005, ApJ, 634, 1214

Lovelace R. V. E., Romanova M. M., Bisnovatyi-Kogan G. S., 1995, MNRAS, 275, 244

Lovelace R. V. E., Romanova M. M., Newman W. I., 2010, MNRAS, 402, 2575

Markwardt C. B., Strohmayer T. E., 2010, ApJ, 717, L149
Markwardt C. B., Swank J. H., 2008, The Astronomer's Telegram, 1728, 1
Matt S., Pudritz R. E., 2005, MNRAS, 356, 167
Matt S. P., Pinzón G., de la Reza R., Greene T. P., 2010, ApJ, 714, 989
Mitsuda K. et al., 1984, PASJ, 36, 741
Morrison R., McCammon D., 1983, ApJ, 270, 119
Ng C., Díaz Trigo M., Cadolle Bel M., Migliari S., 2010, A&A, 522, A96
Papitto A., Di Salvo T., Burderi L., Menna M. T., Lavagetto G., Riggio A., 2007, MNRAS, 375, 971
Papitto A., Di Salvo T., D'Aì A., Iaria R., Burderi L., Riggio A., Menna M. T., Robba N. R., 2009, A&A, 493, L39
Papitto A., Riggio A., Burderi L., di Salvo T., D'Aí A., Iaria R., 2011, A&A, 528, A55
Patruno A., 2010a, PoS (HTRA-IV) 028 (arXiv:1007.1108)
Patruno A., 2010b, ApJ, 722, 909
Patruno A., Altamirano D., Messenger C., 2010a, MNRAS, 403, 1426
Patruno A., Hartman J. M., Wijnands R., Chakrabarty D., van der Klis M., 2010b, ApJ, 717, 1253
Patruno A., Rea N., Altamirano D., Linares M., Wijnands R., van der Klis M., 2009a, MNRAS, 396, L51
Patruno A., Watts A., Klein Wolt M., Wijnands R., van der Klis M., 2009b, ApJ, 707, 1296
Patruno A., Wijnands R., van der Klis M., 2009c, ApJ, 698, L60
Poutanen J., 2006, Advances in Space Research, 38, 2697
Poutanen J., 2008, in Wijnands R., Altamirano D., Soleri P., Degenaar N., Rea N., Casella P., Patruno A., Linares M., eds, AIP Conf. proc. 1068, A decade of accreting X-ray millisecond pulsars, AIP, Melville, p. 77
Poutanen J., Beloborodov A. M., 2006, MNRAS, 373, 836
Poutanen J., Gierliński M., 2003, MNRAS, 343, 1301
Poutanen J., Svensson R., 1996, ApJ, 470, 249
Poutanen J., Ibragimov A., Annala M., 2009, ApJ, 706, L129
Rappaport S. A., Fregeau J. M., Spruit H., 2004, ApJ, 606, 436
Riggio A., Di Salvo T., Burderi L., Menna M. T., Papitto A., Iaria R., Lavagetto G., 2008, ApJ, 678, 1273
Riggio A., Papitto A., Burderi L., di Salvo T., Bachetti M., Iaria R., D'Aì A., Menna M. T., 2011, A&A, 526, A95
Romanova M. M., Ustyugova G. V., Koldoba A. V., Lovelace R. V. E., 2002, ApJ, 578, 420
Romanova M. M., Ustyugova G. V., Koldoba A. V., Lovelace R. V. E., 2004, ApJ, 610, 920
Shakura N. I., Sunyaev R. A., 1973, A&A, 24, 337
Shimura T., Takahara F., 1995, ApJ, 445, 780
Simon J. B., Hawley J. F., Beckwith K., 2011, ApJ, 730, 94
Uzdensky D. A., 2004, Ap&SS, 292, 573
Uzdensky D. A., Königl A., Litwin C., 2002a, ApJ, 565, 1191
Uzdensky D. A., Königl A., Litwin C., 2002b, ApJ, 565, 1205
Viironen K., Poutanen J., 2004, A&A, 426, 985
Wang J. C. L., Sulkanen M. E., Lovelace R. V. E., 1990, ApJ, 355, 38
Wang Y., 1987, A&A, 183, 257
Wijnands R., van der Klis M., 1998, Nat, 394, 344